minerals

MDPI

Article

Effect of Curing Temperature under Deep Mining Conditions on the Mechanical Properties of Cemented Paste Backfill

Yong Wang [1,2,3], Yansen Cao [1,4,*], Chen Cao [1,4,*] and Hongjiang Wang [1,3]

[1] School of Civil and Resource Engineering, University of Science and Technology, Beijing 100083, China
[2] State Key Laboratory for GeoMechanics and Deep Underground Engineering, China University of Mining & Technology, Beijing 100083, China
[3] Key Laboratory of Ministry of Education for Efficient Mining and Safety of Metal Mines, University of Science and Technology, Beijing 100083, China
[4] CINF Engineering Co., Ltd., Changsha 410001, China
* Correspondence: yansencao@126.com (Y.C.); g20208002@xs.ustb.edu.cn (C.C.)

Abstract: Nowadays, the cemented paste backfill mining method is widely used in mines. Since the temperature of the mine increases with increasing mining depth, the influence of temperature on the mechanical properties of cemented paste backfill (CPB) require attention. To address the problem of less research on paste performance in high temperature environments, uniaxial compressive strength tests of CPB at different temperatures were performed, and it was observed that temperature had a significant effect on the CPB strength. The CPB strength at a curing temperature above 40 °C deteriorated in the later curing time period, CPB at 65 °C was "crisp", and the strength was lower than 40 °C in 3~28 days. Microscopic tests, such as thermogravimetric analysis (TGA/DTG), X-ray diffraction (XRD) and scanning electronic microscopy (SEM) analysis, of the samples found that the coarsening of the pore structure of CPB was the main reason for the decrease in the strength caused by the increase in temperature. The effect of curing temperature on the deformation characteristics of CPB was studied. Different curing temperatures had a greater impact on the stress-strain curve and elastic modulus, and there was a linear relationship between the elastic modulus and strength. Finally, based on MATLAB, a back propagation (BP) neural network model of strength under different curing temperature conditions was established. Compared with the actual value and the predicted value, the average absolute error was less than 0.2 MPa, and the average relative error was less than 6%. This prediction model had a high accuracy. The research results provide a good reference significance for the strength design of CPB.

Keywords: cemented paste backfill; curing temperature; mechanical properties; microanalysis; deformation characteristics

check for updates

Citation: Wang, Y.; Cao, Y.; Cao, C.; Wang, H. Effect of Curing Temperature under Deep Mining Conditions on the Mechanical Properties of Cemented Paste Backfill. *Minerals* **2023**, *13*, 383. https://doi.org/10.3390/min13030383

Academic Editor: Abbas Taheri

Received: 29 January 2023
Revised: 20 February 2023
Accepted: 3 March 2023
Published: 9 March 2023

Copyright: © 2023 by the authors. Licensee MDPI, Basel, Switzerland. This article is an open access article distributed under the terms and conditions of the Creative Commons Attribution (CC BY) license (https://creativecommons.org/licenses/by/4.0/).

1. Introduction

After decades of continuous large-scale mining, China's shallow resources have become exhausted [1]. The only way to develop metal mines in the future is to reach the deeper parts of the earth [2]. However, by increasing the mining depth, geological conditions gradually deteriorate. According to geothermal gradient research, the temperature increases by approximately 3 °C for every 100 m. At present, the average ground temperature of global mines more than one kilometer deep is 30~40 °C. When exploring the influence of mining depth on temperature in a gold mine in South Africa, it was found that the average temperature was 35 °C when the depth was 3000 m, 50 °C when the mining depth was 4000 m, and 70 °C when the mining depth was 5000 m [3]. In the Fengyu lead-zinc mine in Japan, although the mining depth is only 500 m, the temperature is as high as 80 °C, due to fissure hot water [4].

The cemented paste backfill (CPB) mining method is widely used to fill the goaf in mines around the world. It can maximize the use of tailings, and has the characteristics of

non-stratification, non-separation and non-dehydration [4–8], which can effectively solve safety and environmental problems. Under deep mining condition, the temperature effect is an important factor in the evolution of paste mechanical properties [9,10]. In underground mines using this method, there are many factors that lead to temperature change, such as different depth and geological conditions of the mine, the hydration reaction in the process of paste hardening, heat generated by friction with the pipe wall in the process of slurry transportation, and various human factors.

Research on the influence of temperature on the mechanical properties of cementitious materials was first carried out in the field of concrete, such as the influence of initial temperature on the mechanical properties of concrete [11–13]. However, paste material is different from concrete, and the conclusions drawn in the concrete field cannot be fully applied to CPB. Therefore, there are also some studies on the effects of initial temperature and curing temperature on the mechanical properties of paste materials. For example, E.G. Thomas [14] studied the relationship between temperature and the strength of CPB. When the temperature is lower than 10 °C, the curing temperature has a great impact on CPB strength, and the low temperature will inhibit the hydration reaction of cement in the filling slurry. Li Xingshang [15] found that CPB strength is greatly affected by the temperature when the cement content is low. The development speed of strength is significantly increased when the curing temperature exceeds 40 °C. Jiang [16] studied the strength rule of CPB with different concentrations of sodium chloride at low temperatures. It was found that CPB strength decreased with increased sodium chloride concentration at low temperatures. Celestin [17] studied the effect of curing temperature on the performance of CPB. It was found that the curing temperature had great impact on the durability, mechanical properties and microstructure of CPB. Pokharel [18] studied the influence of temperature and sulfate on the permeability of CPB, and found that the main factors affecting the permeability of CPB depend on the curing temperature and initial sulfate content. Aldhafeeri [19] studied samples with different curing time and temperature, and found that the strength of CPB was affected by the coupling of curing time and temperature. Wang Yong [20] studied the effect of initial temperature on the mechanical properties of CPB, and found that the law of "strength inverse increase" applied when the initial temperature was 50 °C. Fall [21] studied the effect of curing temperature and different component ratios on the mechanical properties of CPB and found that the strength of CPB will increase with the increase of curing temperature. Wu [22] explored the coupling effect of temperature and the hydration reaction process on the rheological properties of CPB through a mathematical model.

Most of the above studies focus on the effect of initial temperature or medium and low curing temperature on the mechanical properties of CPB. Few studies have been carried out on the mechanical properties of CPB in high-temperature environments. Furthermore, there are few studies on the influence of hydration reaction, microstructure and the strength formation mechanism. Therefore, this paper explores the influence of different curing temperatures on CPB strength, and reveals the influence mechanism of curing temperature on CPB mechanical properties by setting the same temperature as the mine at different depths.

2. Materials and Methods

2.1. Experimental Materials

The materials include tailings, 32.5 Portland cement and water. The tailings came from a lead-zinc ore dressing site in Zhangjiakou, and its particle size distribution is shown in Figure 1. The particle size of tailings less than 20 μm account for 28.09%.

The physical properties and chemical composition of tailings are shown in Tables 1 and 2. It can be seen from Table 2 that the tailings mainly include SiO_2, Fe_2O_3, Al_2O_3, CaO and other components.

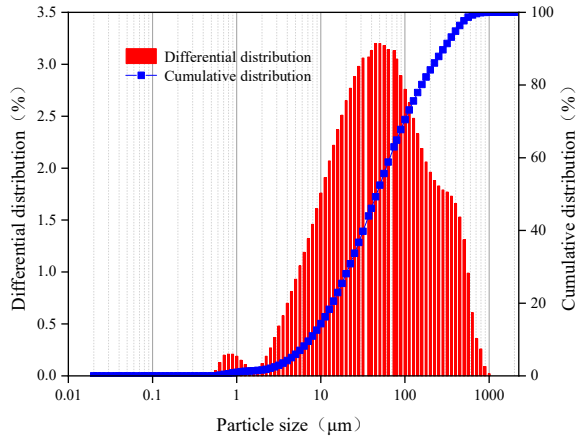


Figure 1. Particle size distribution of tailings.

Table 1. Physical properties of tailings.

Proportion	Average Loose Density/t·m^{-3}	Average Density/t·m^{-3}	Loose Porosity/%	Dense Porosity/%
3.09	1.407	1.653	54.45	46.5
Particle size composition	**D10/μm**	**D25/μm**	**D50/μm**	**D75/μm**
	7.382	17.478	45.949	122.475

Table 2. Mass fraction of main chemical components of tailings (%).

SiO_2	Fe_2O_3	Al_2O_3	CaO	SO_3	MgO
40.8383	21.1618	14.0069	8.1996	5.2409	3.6918

2.2. Experimental Method

2.2.1. Physical Property and Compressive Strength Test

After the tailings were dried, the slurry was made according to a 1:8 ratio of cement to sand and a mass concentration of 72%. The slurry was then injected into molds sized 7.07 cm × 7.07 cm × 7.07 cm. Next, the samples were removed from the molds and moved into a test box with different temperatures. The samples were cured for 3 d, 7 d, 14 d and 28 d under an environment of 95% humidity. The temperature parameters were set at 20 °C, 35 °C, 40 °C, 50 °C and 65 °C. In order to ensure the reliability of the experimental results, three samples were prepared for each group of experiments. The uniaxial compressive strength test was conducted according to GB/T 17671-1999. A sample with a mass of m_1 was dried in an oven at 90 °C for 36 h, and then its mass was weighed again as m_d. The water content w was calculated according to Equation (1).

$$\omega = \frac{m_1 - m_d}{m_d} \tag{1}$$

After obtaining the water content of the samples, the dry density ρ_d was calculated according to Equation (2).

$$\rho_d = \frac{100\rho}{100 + \omega} \tag{2}$$

where ρ is the volume weight of CPB.

2.2.2. Micro-Performance Test Method

Anhydrous ethanol was used to stop the hydration of the samples. The dried samples were cut into small pieces and prepared for scanning electronic microscopy (SEM). Then the samples were ground fine enough to pass through an 80-μm-hole sieve for X-ray diffraction (XRD) analysis and thermogravimetric analysis (TGA/DTG). An SU8200 cold field emission

scanning electron microscope was used for the SEM test, an Ultima-IV X-ray diffractometer for the XRD test, and a DTG-60A thermogravimetric analyzer for TGA/DTG.

3. Results and Discussion

3.1. Evolution Law of Physical Properties at Different Curing Temperatures

The water content and dry density of CPB can reflect the mechanical properties of CPB. The change in water content with curing time at different curing temperatures is shown in Figure 2. It can be seen from Figure 2 that the water content of CPB decreased with increased curing time under different curing temperatures and dropped the fastest in the first seven days. When the temperature was 20 °C, 35 °C, 50 °C and 65 °C, the water content decreased by 3.3%, 3.4%, 4.2% and 4.4%, respectively, after seven days, compared with the water content after three days (calculated by $(w_{3d}\text{-}w_{7d})/w_{3d}$). It can be seen that the higher the curing temperature rose, the faster the water content decreased. The reason for this is that the hydration rate is faster earlier on. With the hydration reaction, more and more free water becomes bound water, and thus, the water content gradually decreases. The higher the curing temperature rose, the faster was the speed of hydration reaction, and at the same time, the lower the water content.

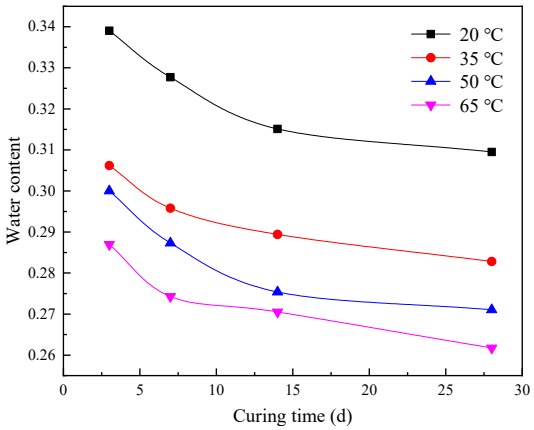


Figure 2. Variation of water content with time at different temperatures.

The change rule of dry density of CPB is shown in Figure 3. Under different curing temperatures, the dry density of CPB increased with the increased curing time, and the growth rate was the fastest in the first 14 d. After 14 d, with the hydration reaction completed, the change in dry density tended to be flat. However, it can be observed that at 28 d, the dry density of CPB at a higher curing temperature was relatively lower, and the dry density at 65 °C was 1.86% lower than that at 20 °C. This indicates that the high temperature will cause the structure of CPB to loosen at 28 d.

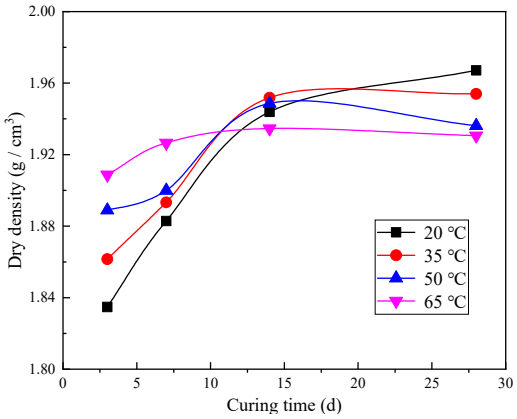


Figure 3. The change in dry density with time at different temperatures.

3.2. Change Law of Uniaxial Compressive Strength under Different Curing Temperatures

3.2.1. Effect of Curing Temperature on the Evolution Trend of Uniaxial Compressive Strength with Curing Time

Figure 4 shows the change of strength with curing time under different curing temperatures. It can be seen that the CPB strength at 20 °C and 35 °C increased with increasing curing time, and the strength at 35 °C was significantly higher than that at 20 °C. After curing for 3 d, 7 d, 14 d and 28 d, the samples' strength at 30 °C was 106%, 55%, 10.7% and 8.5% higher than that at 20 °C, respectively. This is mainly because with the increase in curing time, the hydration process of CPB under different curing temperatures is getting closer. At 40 °C and 50 °C, the CPB strength gradually increased in 14 d, and they reached 2.68 MPa and 3.31 MPa, respectively, at 14 d. However, after 14 d, the strength began to decline to 2.41 MPa and 1.933 MPa, which decreased by 10.2% and 41.6%, respectively. The decline rate at 50 °C was significantly higher than that at 40 °C. For this reason, the higher temperature causes the samples' structure to produce pores, resulting in a decrease in strength. The higher the temperature, the greater the decrease in strength [19]. Razak [23] also believes that there is a threshold value for the effect of temperature on cement solidification. Once the threshold value is exceeded, it is detrimental to the formation of cement hydration. It can also be seen from Figure 4 that at 65 °C, after a certain strength (1.95 MPa) was produced in the first three days, the strength began to decline rapidly. After 14 d, the strength became stable. The strength at 28 d decreased by 52% compared with that at 3 d. This is because the high temperature environment causes the rapid gasification of water in the paste at the early stages of hydration, resulting in a series of pores. This phenomenon is later verified. At 28 d, the sample showed an obvious "crisp" phenomenon, as shown in Figure 5.

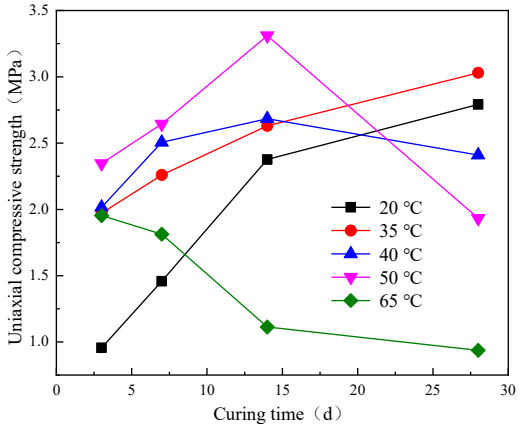


Figure 4. Variation of strength with curing time under different curing temperatures.



Figure 5. Surface morphology of samples at 65 °C for 28 d.

3.2.2. Effect of Curing Temperature on the Strength at the Same Curing Time

The curing temperature had a significant impact on the development of CPB strength. Figure 6 shows the change in CPB strength with temperature under different curing times. It can be seen that the strength increased with increases curing temperature (≤50 °C) at 3 d, 7 d and 14 d. Compared with 20 °C, the strength at 50 °C increased by 145.3%, 81.3% and 39.35%, respectively. It can be considered that within a certain range (≤50 °C), temperature has a greater impact on the increase of early strength.

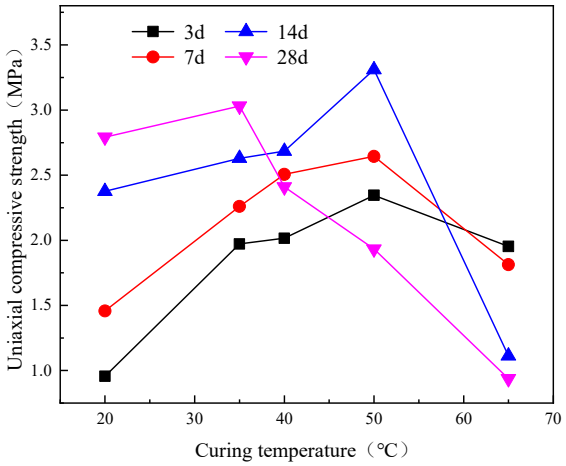


Figure 6. Change in strength with curing temperature at 3 d, 7 d and 14 d.

At 28 d, with the curing temperature increase, the CPB strength reached the maximum (3.03 MPa) at 35 °C, and then began to decline. The fastest decline occurred at 50–65 °C. This shows that the curing temperature had an obvious effect on the 28 d's strength. When the curing temperature is higher than 40 °C, CPB strength begins to deteriorate.

3.3. Microstructure Analysis of CPB under Different Curing Temperatures

3.3.1. Results of TGA/DTG and XRD

Analysis of Results at 20 °C and 50 °C for 3 d

In order to reveal the influence of different curing temperatures on the strength, TGA/DTG and XRD were carried out on the samples at 20 °C and 50 °C for 3 d, as shown in Figure 7. At the temperature ranges of 100–200 °C, 400–550 °C and 650–750 °C, the weight loss and endothermic peak of the samples at 50 °C and 3 d were higher than that at 20 °C and 3 d, respectively, indicating that more C-H-S, ettringite, CH and $CaCO_3$ can be formed at relatively high temperatures.

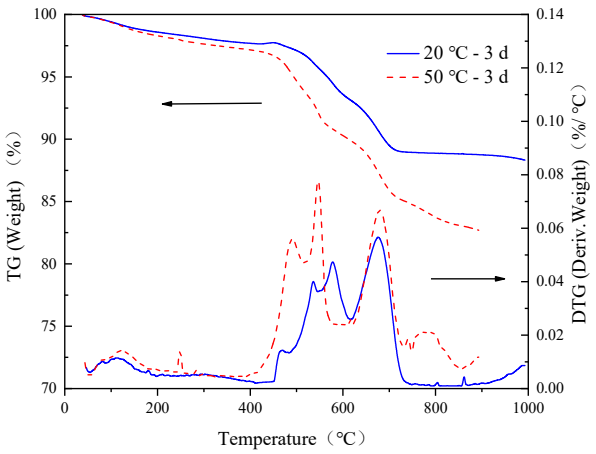
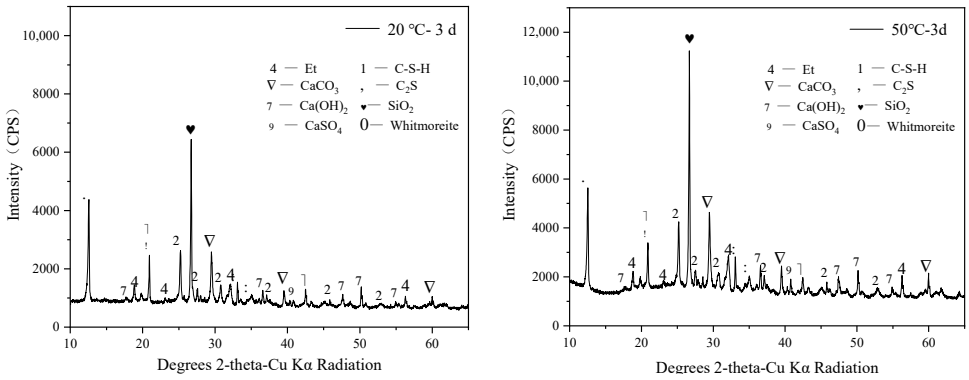


Figure 7. The effect of curing temperature at 20 °C and 50 °C on TGA/DTG for 3 d.

The XRD for samples was further analyzed, as shown in Figure 8. A large amount of C-H-S, ettringite, CH, $CaSO_4$ and $CaCO_3$ were generated from CPB at different curing temperatures. It can be seen from Figure 8 that at the diffraction angle of 18°2-theta, the strength of CH was 1451 CPS at 20 °C and 3d, and 1510 CPS at 50 °C and 3d. Similarly, the CH intensity at the diffraction angle of 47 and 51°2-theta at 50 °C were higher than that at 20 °C. However, the strength of C_2S was decreasing. This shows that the amount of hydration products (CH) increases with the increase of temperature at 3 d.



(**a**) 20 °C (**b**) 50 °C

Figure 8. The effect of different curing temperatures on the XRD at 3 d.

Analysis at 40 °C and 65 °C for 28 d

Compared with 40 °C, the strength of CPB decreased at 65 °C at different curing times, and the curing temperature had a significant impact on the strength at 28 d. When the curing temperature is higher than 40 °C, the CPB strength will deteriorate. In order to explain the cause of deterioration, thermal analysis and XRD analysis were performed on the samples at 40 °C and 65 °C for 28 d, as shown in Figure 9. When the curing temperature was 65 °C and the time 28 d, the weight loss and endothermic peak of samples in the temperature ranges of 100–200 °C and 550–700 °C were higher than that at 40 °C, which indicates that more hydrates can be produced at 65 °C and 28 days.

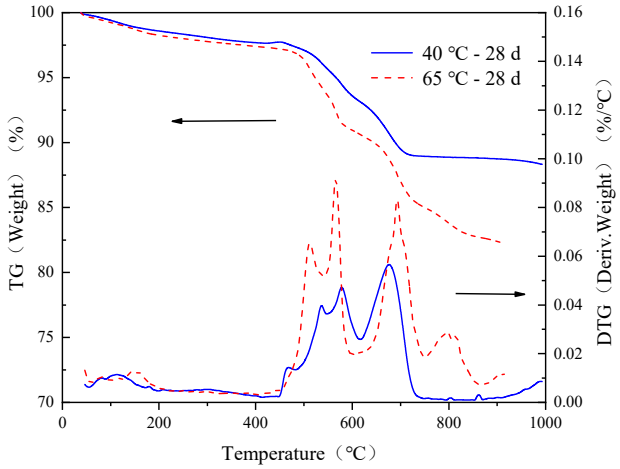
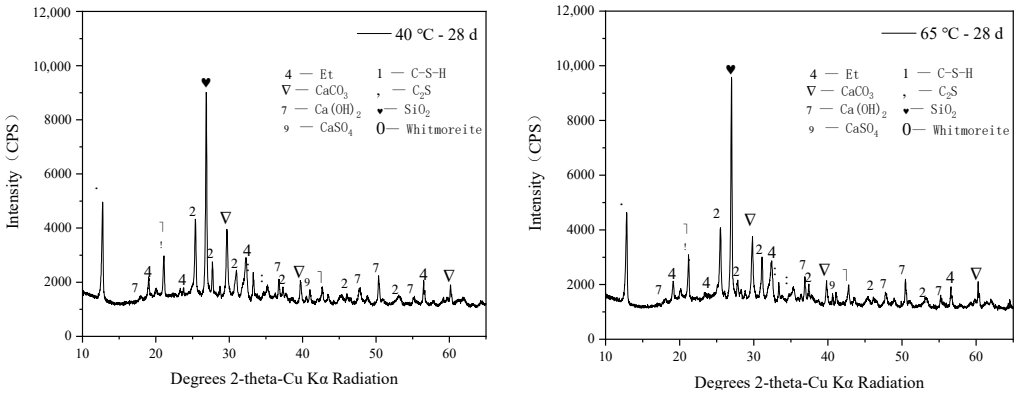


Figure 9. The effect of curing temperature (40 °C and 65 °C) on the TGA/DTA at 28 d.

It can be seen from Figure 10 that at 28d, the strength of CH at 65 °C was 18 (1494CPS), 47 (1508CPS) and 51°2-theta (2236CPS), which was higher than 18 (1470CPS), 47 (1401CPS) and 51°2-theta (2193CPS) at 40 °C. This means that at 28d, the higher the temperature, the more hydration products will be produced, and the higher the strength should be, which is consistent with the thermal analysis results, but contrary to the change law of strength. Therefore, the main factor affecting the strength is not the amount of hydration products.



(**a**) 40 °C (**b**) 65 °C

Figure 10. The effect of different curing temperatures on the XRD at 28 d.

The Consistency of the Results of the Two Analytical Methods

Thermal analysis and XRD analysis explain the main reason why the strength of CPB increased with the increase of temperature at 3 d, 7 d and 14 d: the high temperature accelerates the hydration reaction, and the amount of hydration products (C-S-H, C-H, ettringite and other ingredients) increases with the temperature increase, and these hydration products are beneficial to the CPB strength. This suggests that at 28 d, the amount of hydration products was not the main factor affecting strength change.

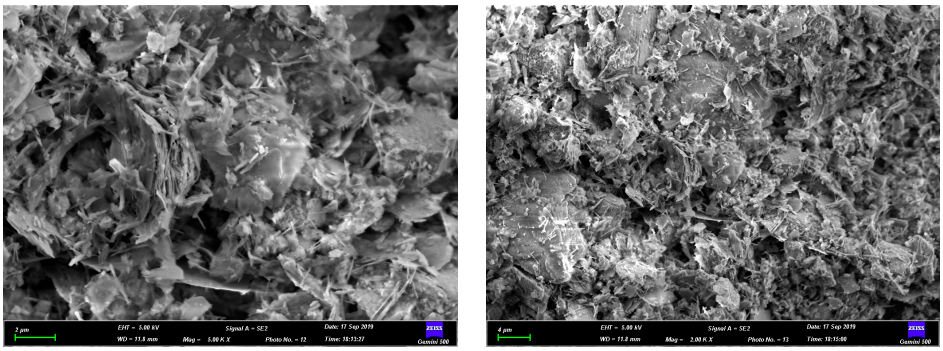
3.3.2. Electron Microscope Scanning and Pore Analysis

The ZEISS Gemini 500 electron microscope equipment (Figure 11) was used to observe samples at 20 °C for 3 d and 28 d.



Figure 11. ZEISS Gemini 500 electron microscope equipment.

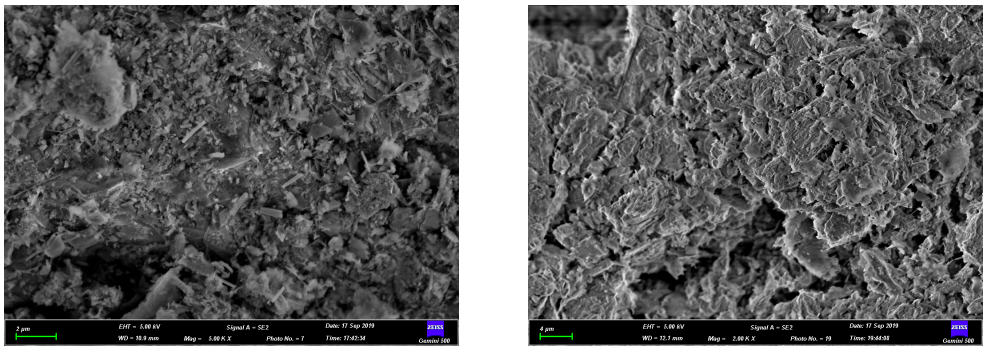
Figure 12 shows the SEM image of the samples at 20 °C and 3 d. It can be seen from Figure 12 that many needle-like ettringite and crystalline CH precipitates were formed inside the samples at 20 °C for 3 d. The interlaced link of acicular ettringite forms a network structure, which is an important reason for the formation of early CPB strength. However, there were still a large number of pores between the CPB particles at this time. This was because the hydration reaction causes water in the pores to be quickly sucked out, and the speed of the pore-water being sucked out is faster than the precipitation speed of the hydration products, leading to the formation of pores [20]. These pores are gradually filled by hydration products with the increase in curing time.



(**a**) ×5000 (**b**) ×2000

Figure 12. SEM images of CPB at different magnifications (20 °C and 3 d).

Figure 13 shows the SEM images of the samples after curing for 28 d at 20 °C and 50 °C. Comparing the electron microscope images at 20 °C for 3 d and 28 d (Figures 12a and 13a), it can be observed that the pores between tailings particles are filled by hydration products at 28 d, and the structure is more compact, which leads to greater strength.



(**a**) 20 °C (**b**) 50 °C

Figure 13. SEM images of samples at 28d under different temperature conditions.

Compared with the SEM images (28 d) at 20 °C and 50 °C, it can be seen that there are many coarse pores in the sample at 50 °C, and the structure is less dense than that at 20 °C. This may be the reason why the strength (28 d) at 50 °C is lower than that at 20 °C.

In order to verify the conjecture on the cause of the strength change, pore analysis was carried out for the above phenomenon. In this paper, the samples' cross-sections were scanned by electron microscope, and the SEM images were processed with Photoshop and Image Pro Plus software to obtain the microstructure information and the change rule of pore.

It can be seen from Figures 14 and 15 that the curing temperature increase to a certain extent (up to 50 °C) leads to the reduction of porosity and the refinement of pore structure at 3 d and 7 d. For the samples with a curing time of 3d, the porosity at 50 °C was 14.77% lower than that at 20 °C, and the average pore diameter was 7.8% lower than that at 20 °C. The porosity at 50 °C for 7 d was 14.29% lower than that at 20 °C, and the average pore diameter was 13.4% lower. This is because within a range ($\leq$50 °C), high curing temperature promotes the hydration of cement which leads to more cement hydration products and a finer cement matrix porosity. This was also confirmed by previous thermal analysis and XRD analysis. However, when the temperature reached 65 °C, the porosity and average pore diameter in 3 d and 7 d were higher than those at curing temperatures less than 65 °C, the porosity was 8.3% and 26.67% higher than that at 50 °C, and the average diameter of pores was 10.6% and 15.3% higher, respectively. In addition, it is particularly

noted that the average pore diameter increased with increased temperature on 28 d. This phenomenon was also confirmed by SEM images.

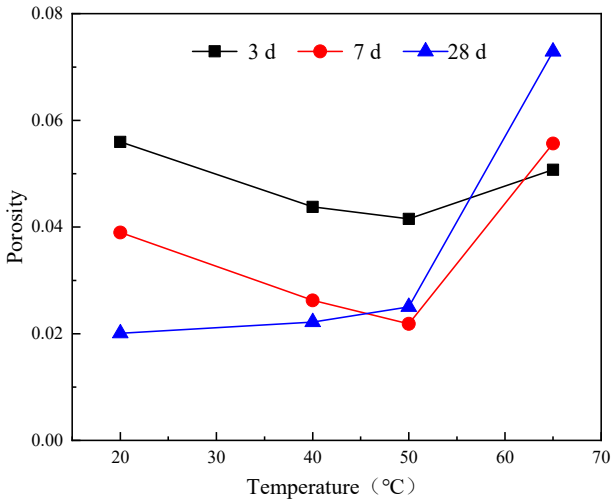


Figure 14. Variation law of porosity of CPB under different curing temperatures.

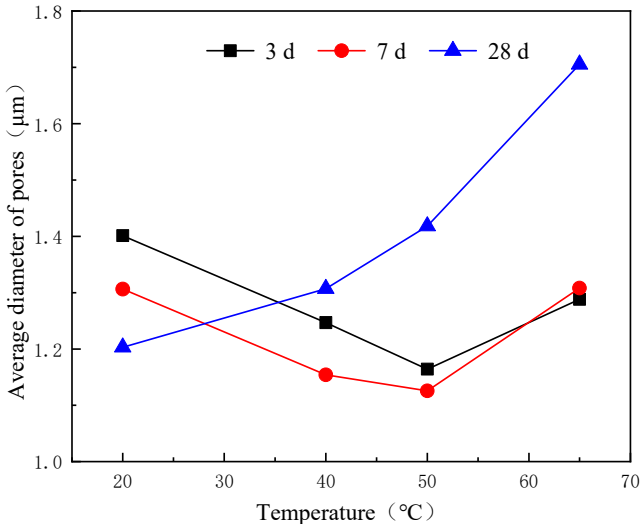


Figure 15. Variation law of average pore diameter of CPB at different curing temperatures.

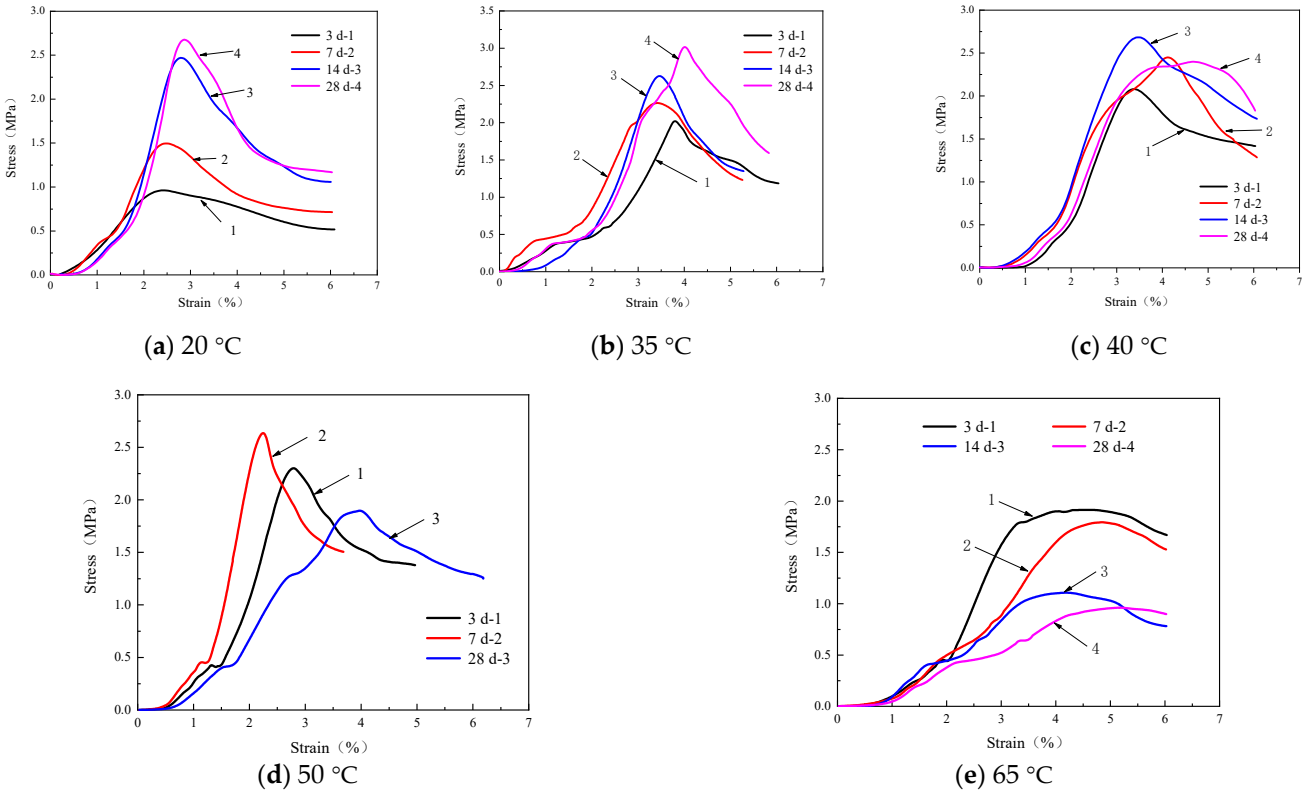
The pore structure of porous media has been considered as an important factor affecting the strength and other properties of cementitious materials [24]. When the temperature is higher than a threshold, the temperature increase will lead to decreased CPB strength. The reason for this is that under the influence of high temperature, the water in CPB at the initial hydration reaction stage is rapidly vaporized, resulting in a series of coarse pores rather than incomplete hydration reaction.

4. Effect of Different Curing Temperatures on Deformation Characteristics of CPB

4.1. Effect of Curing Temperature on the Stress-Strain Curve

The stress-strain curves of CPB under different curing temperatures and curing time are shown in Figure 16. It can be seen that the curing temperature had a great influence on the stress-strain curve. Figure 16 shows the influence of different curing temperatures and time on the deformation behavior of CPB. It can be seen from Figure 16a–d, except for the 28 d's stress-strain curve at 40 °C and 50 °C, that the elastic phase slope of the stress-strain curve gradually increased with increased curing time at each curing temperature. This phenomenon can be attributed to the following: with the increased curing time, the sample produces more hydration products, making it denser, and the same strain requires more

pressure. The abnormal behavior of the 28 d's stress-strain curve at 40 °C and 50 °C is consistent with the change of the corresponding uniaxial compressive strength. Figure 16e shows that at 65 °C, the slope of the elastic stage decreased with the increased curing time. Moreover, the effect on the stress-strain curve was completely opposite compared with the lower temperature. This is because under high temperature conditions, with increased curing time, the vaporization of free water leads to the increase of pore structure, and the peak stress and corresponding strain values decrease simultaneously [25]. At the same time, it can be seen that the strain value corresponding to the peak stress at 35 °C, 40 °C and 50 °C decreased with the temperature increase. At 28 days, the strain value corresponding to the peak stress increased with the temperature increase, indicating that the curing temperature had a great impact on the strain value corresponding to the peak stress. The above results reflect the deformation characteristics of CPB under different curing temperatures.



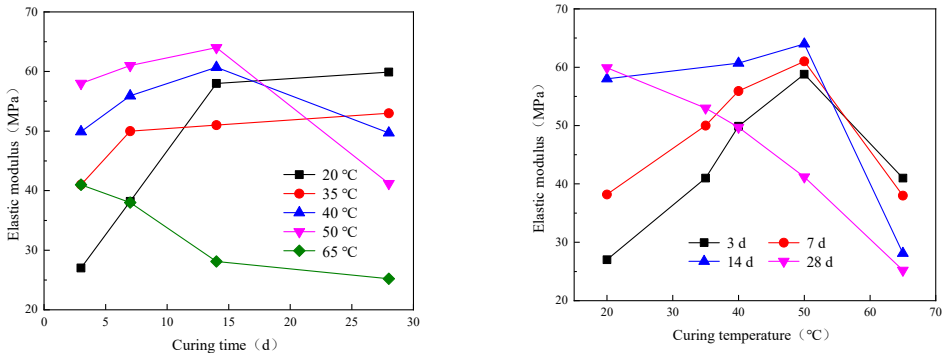
(**a**) 20 °C (**b**) 35 °C (**c**) 40 °C

(**d**) 50 °C (**e**) 65 °C

Figure 16. Stress-strain curves of CPB at different times.

4.2. Effect of Curing Temperature on Elastic Modulus

The effect of different curing temperatures and curing times on the elastic modulus is shown in Figure 17. It can be seen from Figure 17a that curing time had a great impact on the elastic modulus under different curing temperatures. At 20 °C and 35 °C, the elastic modulus value gradually increased with increased curing time, and the increase at 20 °C was significantly higher than that at 35 °C. This is mainly because with the increased curing time, the hydration reaction of cement was gradually completed, and the increase of hydration products led to the increase of hardness. At 40 °C and 50 °C, the elastic modulus gradually increased in 14d. However, after 14d, the elastic modulus began to decline, and the decline rate at 50 °C was significantly higher than that at 40 °C. The reason is that the higher temperature causes CPB to produce more pores, and leads to the decline of mechanical properties. At 65 °C, the elastic modulus continued to decline with increasing curing time. The high temperature caused the rapid hydration reaction of CPB at the initial curing stage, which led to the incomplete hydration of the cement. At the same time, the high temperature will lead to the rapid gasification of moisture in the sample and result in a series of pores, which will affect the mechanical properties of CPB.



(**a**) Effect of curing time (**b**) Effect of curing temperature

Figure 17. Variation law of elastic modulus with different factors.

It can be seen from Figure 17b that curing temperature had a great impact on the elastic modulus of CPB. At 3 d, 7 d and 14 d, the elastic modulus increased with increasing curing temperature when the curing temperature was not more than 50 °C. At 65 °C, the elastic modulus of CPB decreased at different curing times. At 28 d, the elastic modulus continued to decline with the increasing curing temperature. This is because the increase of temperature leads to greater and coarser pore sample structure. The interface between aggregate–cement slurry becomes more porous, and microcracks in the interface area are more likely to occur when pressed. Therefore, the elastic modulus is lower [26].

4.3. Effect of Curing Temperature on the Relationship between Uniaxial Compressive Strength and Elastic Modulus

Figure 18 shows the relationship between elastic modulus and uniaxial compressive strength under different curing temperatures and curing times. It can be seen from Figure 18 that the elastic modulus increases with the increase of uniaxial compressive strength under different curing temperatures, indicating that the effect of curing temperature on the relationship between elastic modulus and uniaxial compressive strength is not obvious.

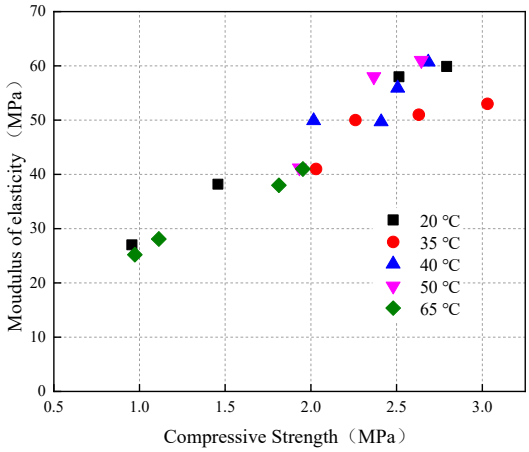


Figure 18. The relationship between elastic modulus and uniaxial compressive strength at different curing temperatures.

The linear regression analysis of the relationship between elastic modulus and uniaxial compressive strength and the square root of uniaxial compressive strength was carried out. The fitting results are shown in Figures 19 and 20, and Equations (3) and (4).

$$E = 18.2559518f + 10.54101 \quad (3)$$

$$E = 48.2156\sqrt{f} - 22.645 \quad (4)$$

where E is the elastic modulus, MPa; f is the uniaxial compressive strength, MPa.

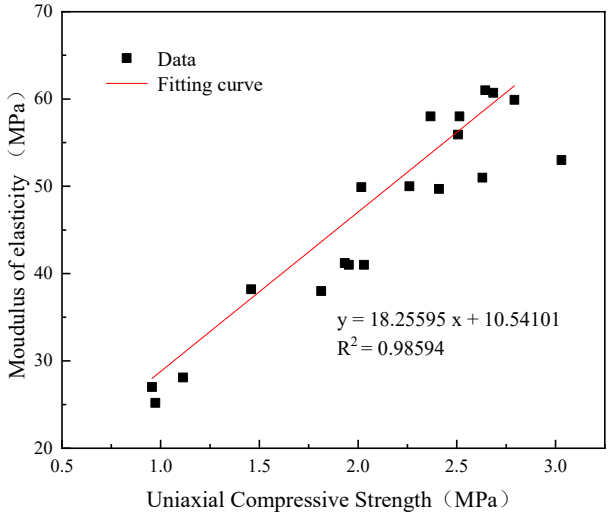


Figure 19. Regression analysis between elastic modulus and uniaxial compressive strength.

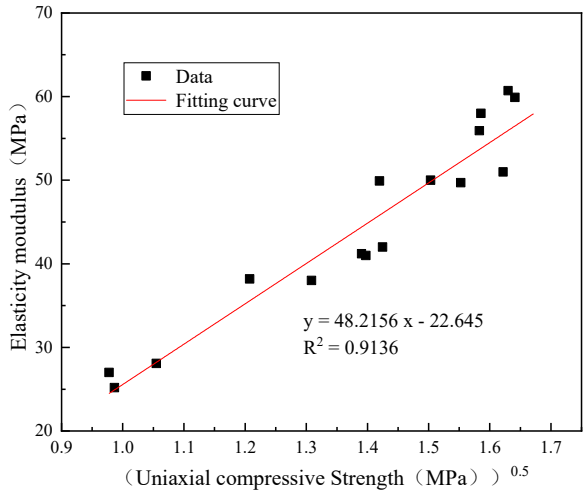


Figure 20. Regression analysis between elastic modulus and square root of uniaxial compressive strength.

The results show that there was a significant linear relationship between elastic modulus and uniaxial compressive strength, and the correlation coefficient was 0.986. The elastic modulus also had a good correlation with the square root of uniaxial compressive strength, with a correlation coefficient of 0.914.

4.4. Strength Prediction Model of CPB under Different Curing Temperatures

In order to predict the CPB strength under different curing temperatures, the nonlinear relationship between temperature and time and uniaxial compressive strength was established based on MATLAB and a BP neural network. The structure of the BP neural network is mainly composed of input layer, hidden layer and output layer [27]. The BP neural network design mainly includes the determination of neural network topology, network parameters and sample data processing [28]. Table 3 shows the samples selected in the process of model establishment. There were 20 groups of experimental data. Fifteen samples were randomly selected as training samples and five samples were validation samples. The structure of the CPB strength prediction model under the influence of different temperatures is shown in Figure 21.

Table 3. CPB strength data under different curing temperatures (MPa).

Time \ Temperature	20 °C	35 °C	40 °C	50 °C	65 °C
3d	0.956	1.972	2.016	2.346	1.953
7d	1.458	2.260	2.506	2.644	1.813
14d	2.376	2.630	2.684	3.310	1.113
28d	2.792	3.030	2.410	1.933	0.937

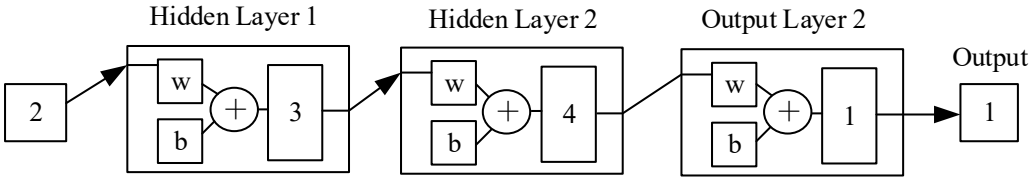


Figure 21. The structure of the CPB strength prediction model under the influence of different temperatures.

Figure 22 and Table 4 show the comparison between the measured and predicted values of strength. It can be seen from Table 4 that the maximum absolute error between the measured value and the predicted value was 0.592 MPa, the average absolute error was 0.084 MPa, the maximum relative error was 24.5%, and the average relative error was 3.7%. It can be seen from Figure 22 that the measured values were close to the predicted values. This shows that the prediction model is highly accurate.

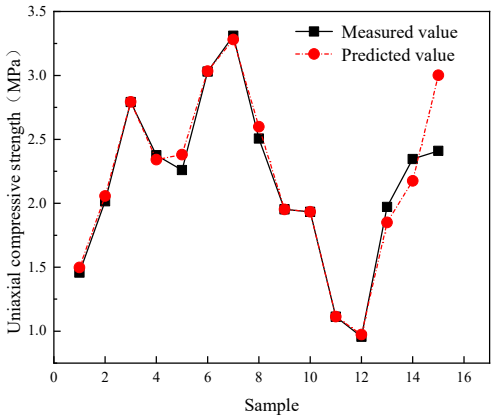


Figure 22. Comparison of measured values and predicted values.

Table 4. Prediction results of strength at different temperatures.

Number	Measured Values/MPa	Predicted Values/MPa	Absolute Error/MPa	Relative Error/%
1	1.458	1.498	−0.040	−2.709
2	2.016	2.058	−0.042	−2.063
3	2.792	2.793	−0.001	−0.039
4	2.376	2.341	0.035	1.465
5	2.26	2.381	−0.121	−5.332
6	3.03	3.034	−0.004	−0.122
7	3.31	3.280	0.030	0.900
8	2.506	2.599	−0.093	−3.703
9	1.953	1.952	0.001	0.046
10	1.933	1.934	0.000	−0.026
11	1.1129	1.114	−0.001	−0.072
12	0.956	0.973	−0.017	−1.778
13	1.972	1.851	0.122	6.161
14	2.346	2.176	0.171	7.268
15	2.41	3.002	−0.592	−24.544
Average value			0.084	3.749

Note: absolute error = measured value–predicted value; relative error = (predicted value–measured value)/measured value.

5. Conclusions

In the process of deep mining, CPB mostly exists under the condition of high temperature. In this paper, the change law of the strength of CPB under different curing temperatures was explored, and its influence mechanism was further analyzed (especially the influence of high temperature). This paper is helpful for the CPB strength design and goaf stability in deep mining.

(1) The uniaxial compressive strength of CPB at different temperatures was tested. Microscopic tests, such as TGA/DTG, XRD and SEM analysis, were carried out. It was observed that different curing temperatures had a significant impact on the development of strength. When the temperature was less than 35 °C, the temperature increased promoted strength development. When the temperature was 40 °C, the CPB strength deteriorated at 28 d, and the higher the curing temperature, the more serious the deterioration of strength. When the curing temperature was 65 °C, the samples became seriously crisp. The temperature increase was the main reason for the coarsening of the CPB pore structure and strength reduction.

(2) In addition to the 28 d's stress-strain curve at 40 °C and 50 °C, the law that the slope of the stress-strain curve in the elastic phase gradually increases with increasing curing time was met at each curing temperature. In addition, the curing temperature had great impact on the strain value corresponding to the peak stress. At 3 d, 7 d and 14 d, the elastic modulus first increased and then decreased with increasing curing temperature. At 28 d, the elastic modulus continued to decrease with the increased curing temperature. This was because the temperature increase led to greater and coarser pore structure in samples, and the interface between aggregate and cement slurry also became more porous. The microcracks in the interface area were more likely to occur under pressure. Linear fitting of curing temperature on the relationship between uniaxial compressive strength and elastic modulus showed that curing temperature had no obvious effect on the relationship between elastic modulus and uniaxial compressive strength, but there was a significant linear relationship between elastic modulus and uniaxial compressive strength.

(3) Based on the MATLAB analysis, 20 groups of experimental data were selected. Fifteen groups were randomly selected as training samples and five groups were validation samples. The BP neural network model of strength under different curing temperatures was established. By comparing the measured value with the predicted value, the average absolute error was less than 0.2 MPa, and the average relative error was less than 6%, indicating that the prediction model had high accuracy.

Author Contributions: Y.W.: writing–original draft, resources, funding acquisition, methodology, supervision.; Y.C.: writing–original draft, conceptualization, investigation, formal analysis.; C.C.: writing–review and editing, investigation, validation.; H.W.: writing–review and editing, investigation, validation. All authors have read and agreed to the published version of the manuscript.

Funding: This research was funded by the National Natural Science Foundation of China (No. 52130404), the State Key Laboratory for GeoMechanics and Deep Underground Engineering, China University of Mining & Technology, Beijing (No. SKLGDUEK2127), the Fundamental Research Funds for the Central Universities (FRF-TP-19-002C2Z) and the Fundamental Research Funds for the Central Universities and the Youth Teacher International Exchange & Growth Program (No. QNXM20220002).

Institutional Review Board Statement: Not applicable.

Informed Consent Statement: Not applicable.

Data Availability Statement: Not applicable.

Conflicts of Interest: The authors declare no conflict of interest.

References

1. Li, X.; Zhou, J.; Wang, S.; Liu, B. Review and practice of deep mining for solid mineral resources. *Chin. J. Nonferrous Met.* **2017**, *27*, 1236–1262.
2. Xi, J. Full Text of General Secretary Xi Jinping's Speech: Struggle to Build a World Power in Science and Technology. Available online: http://www.cast.org.cn/n17040442/n17135960/n17136021/17226246.html.2016 (accessed on 30 May 2016).
3. Rawlins, C.A.; Philips, H.R. Reduction of in mine heat loads. In Proceedings of the 7th International Mine Ventilation Congress, Cracow, Poland, 17–22 June 2001; pp. 381–389.
4. Wu, A.; Yang, Y.; Cheng, H.; Chen, S.; Han, Y. Status and prospects of paste technology in China. *Chin. J. Eng.* **2018**, *40*, 517–525.
5. Henriquez, J.; Simms, P. Dynamic imaging and modelling of multilayer deposition of gold paste tailings. *Min. Eng.* **2009**, *22*, 128–139. [CrossRef]
6. Reid, C.; Bécaert, V.; Aubertin, M. Life cycle assessment of mine tailings management in Canada. *J. Clean. Prod.* **2009**, *17*, 471–479. [CrossRef]
7. Li, S.; Zhao, Z.; Yu, H.; Wang, X. The recent progress China has made in the backfill mining method, Part II: The composition and typical examples of backfill systems. *Minerals* **2021**, *11*, 1362. [CrossRef]
8. Zhao, Y.; Soltani, A.; Taheri, A.; Karakus, M.; Deng, A. Application of slag–cement and fly ash for strength development in cemented paste backfills. *Minerals* **2019**, *9*, 22. [CrossRef]
9. Mbonimpa, M.; Kwizera, P.; Belem, T. Mine backfilling in the permafrost, Part II: Effect of declining curing temperature on the short-term unconfined compressive strength of cemented paste backfills. *Minerals* **2019**, *9*, 172. [CrossRef]
10. Bresson, B.; Meducin, F.; Zanni, H.; Noik, C. Hydration of tricalcium silicate (C 3 S) at high temperature and high pressure. *J. Mater. Sci.* **2002**, *37*, 5355–5365. [CrossRef]
11. Escalante, G.; Sharp, J.H. The microstructure and mechanical properties of blended cements hydrated at various temperatures. *Cem. Concr. Res.* **2001**, *31*, 695–702. [CrossRef]
12. Kim, J.K.; Han, S.H.; Park, S.K. Effect of temperature and aging on the mechanical properties of concrete: Part I. Experimental results. *Cem. Concr. Res.* **2002**, *32*, 1087–1094. [CrossRef]
13. Lothenbach, B.; Winnefeld, F.; Alder, C.; Wieland, E.; Lunk, P. Effect of temperature on the pore solution, microstructure and hydration products of Portland cement pastes. *Cem. Concr. Res.* **2007**, *37*, 483–491. [CrossRef]
14. Thomas, E.G. *Characteristics and Behaviour of Hydraulic Fill Material*; University of Queensland: St Lucia, Australia, 1969.
15. Li, X. *Study on Optimization of Mixing Ratio of Water-Sand Cement Filling Materials*; Kunming University of Science and Technology: Kunming, China, 2005.
16. Jiang, H.; Fall, M. Yield stress and strength of saline cemented tailings in sub-zero environments: Portland cement paste backfill. *Int. J. Min. Process.* **2017**, *160*, 68–75. [CrossRef]
17. Celestin, H.J.C. *Geotechnical Properties of Cemented Paste Backfill and Tailings Liners: Effect of Mix Components and Temperature*; University of Ottawa: Ottawa, ON, Canada, 2008.
18. Pokharel, M.; Fall, M. Combined influence of sulphate and temperature on the saturated hydraulic conductivity of hardened cemented paste backfill. *Cem. Concr. Compos.* **2013**, *38*, 21–28. [CrossRef]
19. Aldhafeeri, Z.; Fall, M.; Pokharel, M.; Pouramini, Z. Temperature dependence of the reactivity of cemented paste backfill. *Appl. Geochem.* **2016**, *72*, 10–19. [CrossRef]
20. Wang, Y. *Initial Temperature-Dependence of Multi-Field Property Correlation and Mechanical Behaviors for Cemented Paste Backfill*; University of Science and Technology Beijing: Beijing, China, 2017.
21. Fall, M.; Célestin, J.C.; Pokharel, M.; Touré, M. A contribution to understanding the effects of curing temperature on the mechanical properties of mine cemented tailings backfill. *Eng. Geol.* **2010**, *114*, 397–413. [CrossRef]
22. Wu, D.; Fall, M.; Cai, S. Coupling temperature, cement hydration and rheological behavior of fresh cemented paste backfill. *Min. Eng.* **2013**, *42*, 76–87. [CrossRef]
23. Hashim, A.R.; Fathollah, S. The effect of heat treatment on the compressive strength of cement-slag mortars. *Mater. Des.* **2011**, *32*, 4618–4628.
24. Roy, D.M.; Gouda, G.R. Porosity-strength relation in cementitious materials with very high strengths. *J. Am. Ceram. Soc.* **1973**, *56*, 549–550. [CrossRef]
25. Su, H.; Song, X.; He, Q. Mechanical properties and energy evolution of cemented tailings backfill at different curing temperatures. *J. Min. Strata Control Eng.* **2023**, *5*, 1–11.
26. Yildirim, H.; Sengul, O. Modulus of elasticity of substandard and normal concretes. *Constr. Build. Mater.* **2011**, *25*, 1645–1652. [CrossRef]
27. Wen, K.; Gao, Q.; Chen, D.; Wang, Y. Orthogonal-BP neural network model for strength of phosphogypsum-based cementitious material backfill. *Ind. Miner. Process.* **2018**, *47*, 60–64+68.
28. Zhao, M. *Prediction of Strength for Recycled Aggregate Thermal Insulation Concrete Based on GA-BP Neural Network*; Taiyuan University of Technology: Taiyuan, China, 2018.

Disclaimer/Publisher's Note: The statements, opinions and data contained in all publications are solely those of the individual author(s) and contributor(s) and not of MDPI and/or the editor(s). MDPI and/or the editor(s) disclaim responsibility for any injury to people or property resulting from any ideas, methods, instructions or products referred to in the content.